Synchronous volcanic eruptions and abrupt climate change ∼17.7 ka plausibly linked by stratospheric ozone depletion

Joseph R. Mcconnell, Andrea Burke, Nelia W. Dunbar, Peter Köhler, Jennie L. Thomas, Monica M. Arienzo, Nathan J. Chellman, Olivia J. Maselli, Michael Sigl, Jess F. Adkins, et al.

Synchronous volcanic eruptions and abrupt climate change ~17.7 ka plausibly linked by stratospheric ozone depletion

Joseph R. McConnell[a,1], Andrea Burke[b], Nelia W. Dunbar[c], Peter Köhler[d], Jennie L. Thomas[e], Monica M. Arienzo[a], Nathan J. Chellman[a], Olivia J. Maselli[a], Michael Sigl[a], Jess F. Adkins[f], Daniel Baggenstos[g], John F. Burkhart[h], Edward J. Brook[i], Christo Buizert[i], Jihong Cole-Dai[j], T. J. Fudge[k], Gregor Knorr[d], Hans-F. Graf[l], Mackenzie M. Grieman[m], Nels Iverson[c], Kenneth C. McGwire[n], Robert Mulvaney[o], Guillaume Paris[f], Rachael H. Rhodes[i,p], Eric S. Saltzman[m], Jeffrey P. Severinghaus[g], Jørgen Peder Steffensen[q], Kendrick C. Taylor[a], and Gisela Winckler[r]

[a]Division of Hydrologic Sciences, Desert Research Institute, Reno, NV 89512; [b]School of Earth and Environmental Sciences, University of St. Andrews, St. Andrews, KY16 9AL United Kingdom; [c]New Mexico Institute of Mining and Technology, Socorro, NM 87801; [d]Alfred-Wegener-Institut Helmholtz-Zentrum für Polar- und Meeresforschung, 27512 Bremerhaven, Germany; [e]Sorbonne Université, Pierre and Marie Curie University, Université Versailles St-Quentin, CNRS, Institut National des Sciences de l'Univers, Laboratoire Atmosphères, Milieux, Observations Spatiales, Institut Pierre Simon Laplace, 75252 Paris, France; [f]Division of Geological and Planetary Sciences, California Institute of Technology, Pasadena, CA 91125; [g]Scripps Institution of Oceanography, University of California, San Diego, La Jolla, CA 92093; [h]Department of Geosciences, University of Oslo, NO-0316 Oslo, Norway; [i]College of Earth, Ocean, and Atmospheric Sciences, Oregon State University, Corvallis, OR 97331; [j]Department of Chemistry and Biochemistry, South Dakota State University, Brookings, SD 57007; [k]Department of Earth and Space Sciences, University of Washington, Seattle, WA 98195; [l]Centre for Atmospheric Science, University of Cambridge, Cambridge, CB2 3EN United Kingdom; [m]Department of Earth System Science, University of California, Irvine, CA 92617; [n]Division of Earth and Ecosystem Sciences, Desert Research Institute, Reno, NV 89512; [o]British Antarctic Survey, Cambridge, CB3 OET United Kingdom; [p]Department of Earth Sciences, University of Cambridge, Cambridge, CB2 3EQ United Kingdom; [q]Centre for Ice and Climate, University of Copenhagen, Copenhagen, DK-1017 Denmark; and [r]Lamont-Doherty Earth Observatory, Earth Institute at Columbia University, Palisades, NY 10964

Edited by Wallace S. Broecker, Columbia University, Palisades, NY, and approved August 7, 2017 (received for review April 5, 2017)

Glacial-state greenhouse gas concentrations and Southern Hemisphere climate conditions persisted until ~17.7 ka, when a nearly synchronous acceleration in deglaciation was recorded in paleoclimate proxies in large parts of the Southern Hemisphere, with many changes ascribed to a sudden poleward shift in the Southern Hemisphere westerlies and subsequent climate impacts. We used high-resolution chemical measurements in the West Antarctic Ice Sheet Divide, Byrd, and other ice cores to document a unique, ~192-y series of halogen-rich volcanic eruptions exactly at the start of accelerated deglaciation, with tephra identifying the nearby Mount Takahe volcano as the source. Extensive fallout from these massive eruptions has been found >2,800 km from Mount Takahe. Sulfur isotope anomalies and marked decreases in ice core bromine consistent with increased surface UV radiation indicate that the eruptions led to stratospheric ozone depletion. Rather than a highly improbable coincidence, circulation and climate changes extending from the Antarctic Peninsula to the subtropics—similar to those associated with modern stratospheric ozone depletion over Antarctica—plausibly link the Mount Takahe eruptions to the onset of accelerated Southern Hemisphere deglaciation ~17.7 ka.

climate | deglaciation | volcanism | ozone | aerosol

Long-term variations in global climate, such as the glacial/interglacial cycles recorded in paleoarchives, are linked to changes in Earth's orbital parameters and insolation (1). Superimposed on this smooth, orbital-scale variability are abrupt changes in climate, resulting in substantial variations among glacial terminations (2) and suggesting that the evolution of each deglaciation may be influenced by climate drivers specific to that deglaciation (3). One such rapid change during the last termination began ~17.7 ky before 1950 (17.7 ka), when paleoclimate records show sharp, nearly synchronous changes across the Southern Hemisphere (SH) such as a widespread retreat of glaciers in Patagonia (4, 5) and New Zealand (6), onset of rapid lake expansion in the Bolivian Andes (7), increases in summertime precipitation in subtropical Brazil (8), decreases in southern Australian aridity (9), and dust deposition recorded in ocean sediment cores (9, 10) (Fig. 1). At the same time, Antarctic ice cores record a sharp decrease in SH continental dust (11), a widespread decline in sea salt deposition, a marked upturn in water isotopic ratios indicating warming (12, 13), and a trend of increasing atmospheric methane (CH_4) (12) and carbon dioxide (CO_2) (14, 15) coincident with a drop in the stable carbon isotopic ratios in CO_2 (14) (Fig. 1). Although the causes are not certain, many of these rapid changes have been attributed to a sudden poleward shift in the westerly winds encircling Antarctica, with resulting changes in SH hydroclimate, sea ice extent, ocean circulation (6, 7, 9), and ventilation of the deep Southern Ocean (16).

The new very high time resolution West Antarctic Ice Sheet (WAIS) Divide (WD) (12) ice core record from West Antarctica (*Materials and Methods*) shows that, following a long period of relative stability extending glacial-state climate conditions [>10 ky after

Significance

Cold and dry glacial-state climate conditions persisted in the Southern Hemisphere until approximately 17.7 ka, when paleoclimate records show a largely unexplained sharp, nearly synchronous acceleration in deglaciation. Detailed measurements in Antarctic ice cores document exactly at that time a unique, ~192-y series of massive halogen-rich volcanic eruptions geochemically attributed to Mount Takahe in West Antarctica. Rather than a coincidence, we postulate that halogen-catalyzed stratospheric ozone depletion over Antarctica triggered large-scale atmospheric circulation and hydroclimate changes similar to the modern Antarctic ozone hole, explaining the synchronicity and abruptness of accelerated Southern Hemisphere deglaciation.

Author contributions: J.R.M. designed research; J.R.M., A.B., N.W.D., P.K., J.L.T., M.M.A., N.J.C., O.J.M., M.S., J.F.A., D.B., J.F.B., E.J.B., J.C.-D., T.J.F., G.K., M.M.G., N.I., K.C.M., R.M., G.P., R.H.R., E.S.S., J.P. Severinghaus, J.P. Steffensen, K.C.T., and G.W. performed research; J.R.M. contributed new reagents/analytic tools; J.R.M., A.B., N.W.D., P.K., J.L.T., M.S., E.J.B., C.B., J.C.-D., G.K., H.-F.G., N.I., K.C.M., and G.W. analyzed data; and J.R.M., A.B., N.W.D., P.K., J.L.T., E.J.B., C.B., H.-F.G., and G.W. wrote the paper.

The authors declare no conflict of interest.

This article is a PNAS Direct Submission.

Freely available online through the PNAS open access option.

Data deposition: The data reported in this work have been deposited with the U.S. Antarctic Program Data Center, www.usap-dc.org/view/dataset/601008.

[1]To whom correspondence should be addressed. Email: Joe.McConnell@dri.edu.

This article contains supporting information online at www.pnas.org/lookup/suppl/doi:10.1073/pnas.1705595114/-/DCSupplemental.

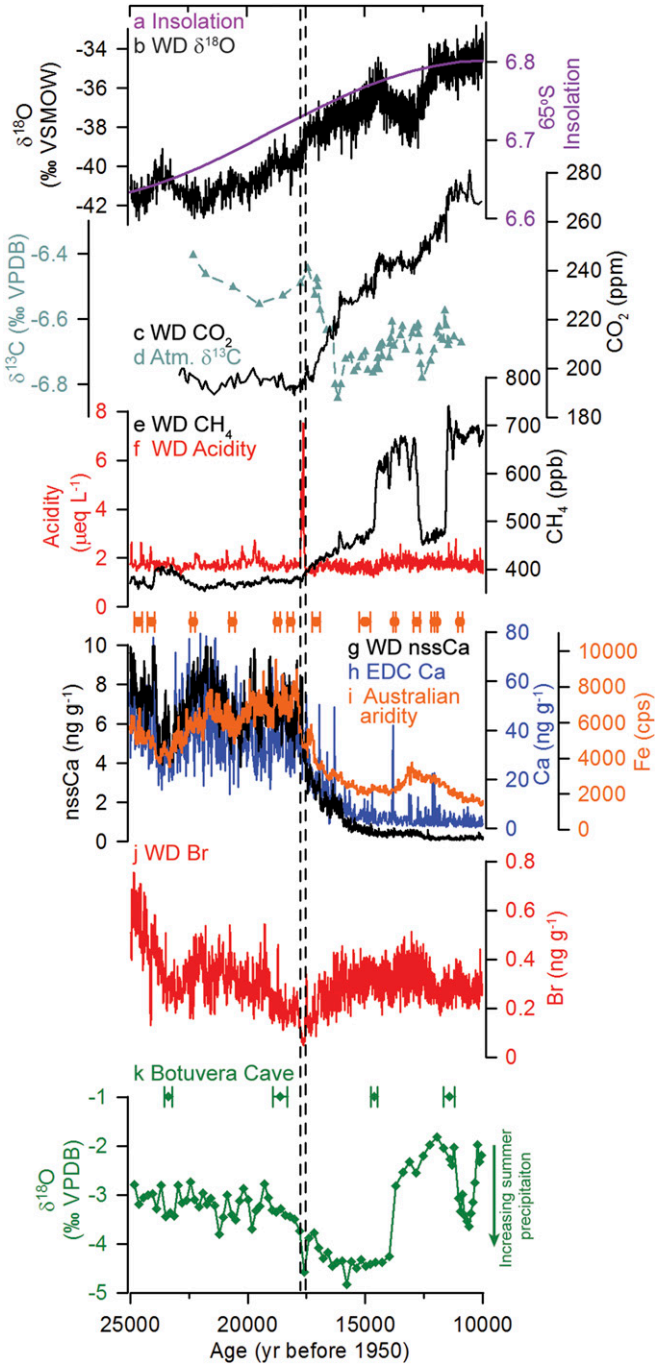

Fig. 1. Changes in climate indicators during the last glacial termination relative to the 17.7 ka glaciochemical anomaly. Shading shows the ∼192-y glaciochemical anomaly. (*A*) Annually integrated (12) 65°S insolation and (*B*) WD $\delta^{18}O$ (12); (*C*) WD CO_2 (15) and (*D*) Taylor Glacier $\delta^{13}C$ of CO_2 synchronized to the WD CO_2 record (46); (*E*) WD CH_4 (60) and (*F*) WD mineral acidity; SH dust proxies (*G*) nssCa in the WD core, (*H*) Ca in the European Project for Ice Coring in Antarctica Dome C (EDC) (11) synchronized to WD using volcanic events, and (*I*) Fe in a South Australian ocean sediment core (9); (*J*) the surface UV indicator Br in the WD core; and (*K*) Botuvera speleothem $\delta^{18}O$ that is a proxy for summertime precipitation in southeastern Brazil (8).

the 65°S annually integrated insolation minimum marking the Last Glacial Maximum (LGM)], sea salt and SH continental dust aerosol concentrations, snowfall rates, water isotope ratios, and greenhouse gas concentrations [CO_2 (15), CH_4] changed at 17.7 ka or soon after, sharply at first and then more gradually (Fig. 1). Concentrations of the traditional continental dust tracer non-sea-salt calcium (nssCa) dropped 100-fold, from ∼7 ng·g^{-1} during the LGM to ∼0.07 ng·g^{-1} during the early Holocene, with nearly 50% of the total decrease occurring during the 400 y after 17.7 ka. Sea-salt sodium concentration (ssNa), thought to be a proxy for sea ice formation, decreased fivefold during the deglaciation, with ∼40% of the decline occurring in this same period (12). About 25% of the ∼8‰ $\delta^{18}O$ and 10% of the 320 parts-per-billion CH_4 overall increases from LGM to the early Holocene values happened during these 400 y (12) (Fig. 1).

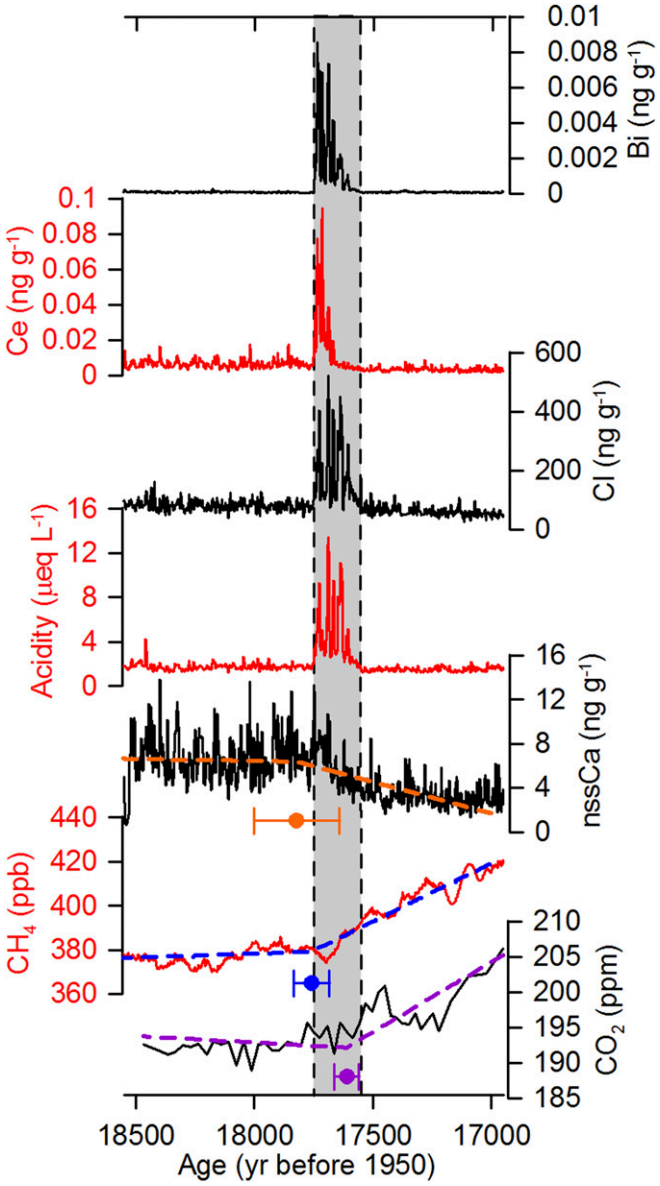

Fig. 2. Selected high-resolution elemental and gas phase measurements through the ∼192-y glaciochemical anomaly in the WD ice core at 17.7 ka (gray shading) showing nine distinct pulses. Acidity, low-boiling-point heavy metals (e.g., Bi), and halogens (e.g., Cl) other than Br (Fig. 1) were highly elevated throughout the anomaly (*SI Appendix*, Fig. S1), with REE (e.g., Ce) enhanced only during the first ∼120 y. SH dust indicators (e.g., nssCa) were elevated only slightly, and slowly increasing greenhouse gas [CH_4 (60), CO_2 (15)] concentrations accelerated during the event (Fig. 1). Measurements in the Byrd core are similar (*SI Appendix*, Fig. S2). Calculated break points (1σ uncertainty) suggest that long-term changes in nssCa, CH_4, and CO_2 concentrations in the WD core began during the 17.7 ka anomaly (*Materials and Methods*).

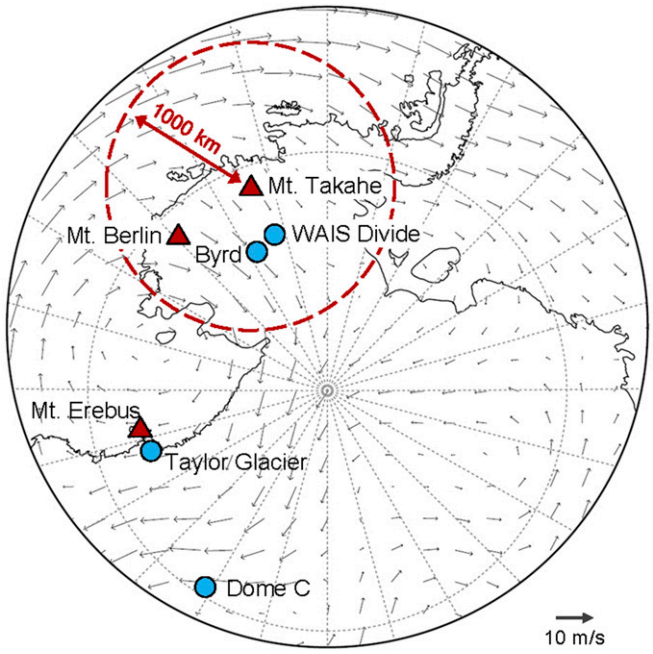

Fig. 3. Spatial extent of the glaciochemical anomaly. Evidence of the ~192-y anomaly has been found >2,800 km from Mount Takahe in ice core (circles) chemical records (*SI Appendix*, Fig. S3) as well as radar surveys from much of West Antarctica. Also shown are area volcanoes (triangles). September/October horizontal wind vectors at 600 hPa based on 1981–2010 National Centers for Environmental Prediction reanalysis fields show transport patterns consistent with observations.

Measurements of nssCa and other SH dust proxies in the WD core (Figs. 1 and 2) (*SI Appendix*, Fig. S1)—complemented by new measurements (Dataset S1) in archived samples of the Byrd core (17) located 159 km from WD (Fig. 3) (*SI Appendix*, Fig. S2)—indicate that the abrupt climate change started in central West Antarctica ~17.7 ka, with the sharp and sustained decline in SH continental dust deposition (Fig. 1) nearly synchronous (*SI Appendix*, *Continuous Ice Core Measurements*) with the start of marked increases in CH_4 and CO_2 (Fig. 2). Starting ~60 (±18) y before the abrupt drop in dust and extending ~132 y after was a unique, long-lived glaciochemical anomaly originally detected in limited discrete measurements of acidity, chloride, and fluoride in the Byrd core (17) (*SI Appendix*, Fig. S3). New continuous measurements of a broad range of elements and chemical species in the WD and Byrd cores (*SI Appendix*, Figs. S1 and S2) show that the glaciochemical anomaly consisted of nine pulses measured between 2,426.97 m and 2,420.04 m depth in the WD core, corresponding to a ~192-y period from 17.748 ka to 17.556 ka (Fig. 2) on the WD2014 timescale (18). Evidence of this glaciochemical anomaly also has been traced throughout West Antarctica and parts of East Antarctica in ice cores (17) (Fig. 3) (*SI Appendix*, Fig. S3) and radar surveys (19).

Mount Takahe 17.7 ka Volcanic Event

Elements and chemical species associated with seawater (e.g., sodium, magnesium, calcium, strontium), fallout from biomass burning (e.g., black carbon, ammonium, nitrate), and continental dust (e.g., aluminum, calcium, vanadium, iron, rubidium, barium) showed little or no change during the glaciochemical anomaly in both the WD and Byrd cores (*SI Appendix*, Figs. S1 and S2). Other elements increased by up to 50 times background concentrations, however, including rare earth elements (REE) that normally are associated with insoluble particles and low-boiling-point heavy metals linked, in past studies, to Antarctic volcanic emissions (20). Concentration changes differed between elements (*SI Appendix*, Figs. S1 and S2), with increases above background levels during nine distinct pulses of 1.7-fold for sulfur; up to sixfold for chlorine; 10-fold for lead; 20-fold for cerium, lanthanum, and thallium; and 50-fold for bismuth. While no increases were observed in the smaller (0.8 μm to 2.4 μm) insoluble particle size fraction, 2.5- and 11-fold increases were found for the medium (2.4 μm to 4.5 μm) and larger (4.5 μm to 9.5 μm) fractions, respectively (*SI Appendix*, Fig. S1). Of all of our ~35 chemical measurements, only bromine and bromide concentrations (*SI Appendix*, *Bromine and Bromide*) declined during this ~192-y period (Fig. 1) (*SI Appendix*, Figs. S1 and S2).

Consistent with the initial interpretation of the original Byrd measurements (17) but in contrast to subsequent interpretations (21) (*Materials and Methods*), the very pronounced enrichments of low-boiling-point heavy metals (20) and halogens (22), as well as elevated concentrations of medium and larger insoluble particle fractions in the WD core (Fig. 2) (*SI Appendix*, Fig. S1), clearly indicate a volcanic source for the glaciochemical anomaly (23). Although sulfur during the anomaly was relatively low (Fig. 4), the S/Cl mass ratio was ~0.1, which is nearly identical to the 0.095 ratio reported for modern emissions from nearby Mount Erebus (23). Moreover, tephra particles from the anomaly (*Materials and Methods*), analyzed by electron microprobe, showed mineralogy of a trachytic volcanic eruption (*SI Appendix*, Table S1) geochemically consistent with tephra from nearby Mount Takahe (24, 25) (76.28°S, 112.08°W), a recently active, flat-topped stratovolcano in West Antarctica located 360 km north of the WD coring site (Fig. 3). Therefore, we refer to the ~192-y series of volcanic eruptions as the "17.7 ka Mount Takahe Event." Estimates of emissions from Mount Takahe from enhancements in chlorine fluxes measured in the WD, Byrd, and Taylor Glacier cores, as well as radar-based evidence on the extent of the fallout plume (Fig. 3), suggest that average and peak chlorine emissions were ~100 $Gg{\cdot}y^{-1}$ and ~400 $Gg{\cdot}y^{-1}$, respectively (*SI Appendix*, *Mt. Takahe Emission Estimates*). These levels are ~10 and ~40 times higher than modern emissions estimated for Mount Erebus (23), as well as ~0.4 and ~1.6 times those reported for Mount Etna, currently the largest point source of chlorine on Earth (22). We estimate that transport of only 1% of the 17.7 ka Mount Takahe emissions to the high-latitude SH stratosphere would have yielded chlorine concentrations comparable to those responsible for modern chlorofluorocarbon-driven ozone depletion.

All of our measurements in the WD, Byrd, and Taylor Glacier (*Materials and Methods*) cores clearly indicate that the 17.7 ka

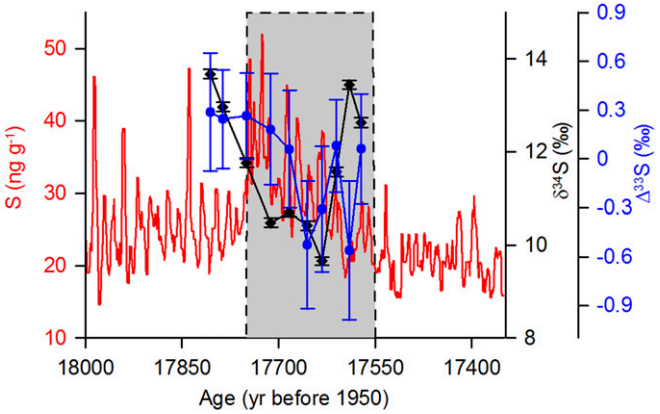

Fig. 4. Sulfur isotope anomalies indicate changes in UV radiation during the 17.7 ka event. Despite relatively modest increases in sulfur concentration in both the WD and Byrd records, volcanic sulfur emissions led to decreased $\delta^{34}S$, while increased UV radiation resulted in anomalous $\Delta^{33}S$. Uncertainties are 2σ.

event resulted from a series of massive halogen-rich, volcanic eruptions in West Antarctica (Figs. 1 and 2) (*SI Appendix*, Figs. S1–S3). Explosive volcanic eruptions inject large amounts of sulfur and other aerosols, often including halogens, into the stratosphere, frequently leading to stratospheric ozone depletion even for small eruptions (26–28) and to an increase in UV radiation at Earth's surface. Photolysis and precipitation scavenging at warmer, lower-latitude sites limit atmospheric lifetimes of volcanic halogens and thus the impacts on stratospheric ozone, although transport of even a small fraction of halogen emissions to the stratosphere can deplete ozone (29). Halogen lifetimes during the 17.7 ka event, however, were extended at Mount Takahe by the extremely cold and dry LGM conditions, particularly during dark winter months. Such a massive and persistent (~192-y) series of halogen-rich volcanic eruptions is unique within the ~68-ky WD ice core record, and the event straddles the most significant abrupt climate change recorded in Antarctic ice cores and other SH climate proxies during the >10-ky period of the last deglaciation (Figs. 1 and 2) which occurred many thousands of years after the 65°S LGM insolation minimum. The probability that these two unique events coincided by chance is the product of the two individual probabilities, and on the order of one in a million. Rather than a highly improbable coincidence, we hypothesize that these massive halogen-rich eruptions are linked causally, by stratospheric ozone depletion, to large-scale changes in SH climate and related changes in atmospheric and oceanic circulation analogous to those from modern, halogen-catalyzed ozone depletion.

Evidence for Stratospheric Ozone Depletion

Evidence for ejection of volcanic material from the 17.7 ka Mount Takahe Event into the stratosphere and/or enhanced tropospheric UV radiation was found in sulfur isotope anomalies in the WD and Byrd cores (Fig. 4). Sulfur concentrations during the ~192-y event were 1.7 times higher than background, and $\delta^{34}S$ values were lower, indicating a volcanic source of the elevated sulfur, since background marine and volcanic sources have $\delta^{34}S$ signatures of 15 to 21‰ and 0 to 5‰, respectively (30). Furthermore, exposure to UV radiation, such as when volcanic sulfur is ejected into the stratosphere above the ozone layer, generates distinct changes in sulfur isotope mass-independent fractionation (MIF; expressed as nonzero values of $\Delta^{33}S$). Previous studies have shown that MIF from a single eruption into the stratosphere follows a distinct evolution from positive to negative $\Delta^{33}S$ during the course of sulfate deposition (31), so low-resolution sampling and multiple overlapping explosive events may result in small values of $\Delta^{33}S$ even for stratospheric eruptions. The $\Delta^{33}S$ of sulfate from before the 17.7 ka event was within 2σ uncertainty of zero, as expected for nonstratospheric sulfate (31, 32). The nonzero $\Delta^{33}S$ measured in the ice during the 17.7 ka event indicated that the volcanic sulfur was indeed bombarded by enhanced UV radiation, either in the stratosphere as a result of ejection above the ozone layer and/or in the troposphere after significant stratospheric ozone depletion. The resolution of the WD and Byrd samples, the multiple explosive phases of the Mount Takahe eruptions, and the low concentration of volcanic sulfur above background levels, however, meant that the magnitude of the MIF anomaly was significant outside of 2σ only for a few samples (*Materials and Methods*).

Evidence for stratospheric ozone depletion and enhanced near-surface UV radiation also comes from changes in bromine concentration in the WD and Byrd ice core records. Photochemical reactions in near-surface snow cause rapid cycling between the snow and air for a broad range of reactive and volatile chemical species, including bromine and nitrate, and a net loss in the snow through time, known as reversible deposition (33, 34). The magnitude of this loss primarily depends on the duration and intensity of exposure of the snow to UV radiation, with duration determined by the burial rate (*SI Appendix*, *Evidence for Reversible Bromine Deposition in Antarctic Snow*), since light penetration below ~0.3 m in the snowpack is much reduced and exposure intensity is determined by the level of impinging UV radiation. During 27 ka to 6 ka in the WD record, there were only two sustained declines in bromine concentration, and the longest and most pronounced decline exactly coincided with the 17.7 ka Mount Takahe Event (Fig. 1). Annual layering in fine insoluble dust particle concentrations in the WD record indicates that the snowfall rate did not change during this period, eliminating burial rate variations as the cause of the bromine decline and implicating increased surface UV radiation (*SI Appendix*, *Snowpack Modeling*).

While bromine release from the snowpack is sensitive to changes in UV radiation, and that sensitivity increases with snow acidity (33), photochemical model simulations as well as examination of the WD record show that acidity alone is not sufficient to explain the observed bromine depletion. First, bromine concentrations in the WD and Byrd cores remained low even during periods between the nine volcanic pulses of the 17.7 ka Mount Takahe Event when concentrations of nearly all elements and chemical species, including acidity, returned to near-background concentrations (*SI Appendix*, Figs. S1 and S2). WD snow accumulation was relatively high (>100 $kg \cdot m^{-2} \cdot y^{-1}$) during this period (18), so the regions of high acidity in the core were well separated from regions of low acidity. Second, consistent with modern observations in which some but not all volcanic eruptions are associated with ozone depletion (26), evaluation of the 100 highest acidity events (annual average concentration >3.0 $\mu eq \cdot L^{-1}$) in the 10 ka to 25 ka WD record shows that 30% were not associated with bromine depletion and that depletion was not proportional to acidity (*SI Appendix*, Fig. S6). This clearly demonstrates that acidity alone did not lead to bromine depletion and suggests that both increased acidity and increased UV radiation were required, as predicted by modeling (*SI Appendix*, *Snowpack Modeling*).

It is unclear whether modern ozone depletion and enhanced surface UV have resulted in bromine depletion in near-surface snow. First, modern chlorofluorocarbon-driven ozone depletion largely has been confined to spring, while volcanically driven Mount Takahe ozone depletion may have persisted throughout the austral summer when the impact on snowpack photochemistry was greater. Second, there was no recent increase in acidity in Antarctic snow, so the sensitivity of bromine reemission to enhanced UV radiation was low. Third, no suitable Antarctic ice core record of bromine was available to assess the modern period (*SI Appendix*, *Comparisons to Modern Ozone Depletion*).

Plausible Linkages to Rapid SH Deglaciation

Observations and climate model simulations indicate that modern anthropogenic ozone depletion is linked to surface climate changes throughout the SH substantially similar to those ~17.7 ka, as documented in paleoclimate archives. These include a poleward shift and acceleration of the westerly winds around Antarctica (35), acceleration of midlatitude easterly winds (35), and southward expansion of the summertime Hadley cell, leading to changes in temperature and precipitation extending from the Antarctic Peninsula (36) to the subtropics, especially during austral summer (37). Specific climate changes include subtropical moistening and midlatitude drying (37) (Fig. 5), as well as pronounced warming in the northern Antarctic Peninsula and Patagonia, with cooling over the Antarctic continent, particularly in East Antarctica (35). Enhanced deep-ocean ventilation around Antarctica with reduction in oceanic uptake of CO_2 (38) also is associated with these modern changes in the westerlies. Quasi-equilibrium simulations of the potential impacts of a sustained ozone hole at 17.7 ka using a coupled Atmosphere Ocean General Circulation Model (AOGCM) initialized to LGM conditions predict qualitatively similar responses compared with the

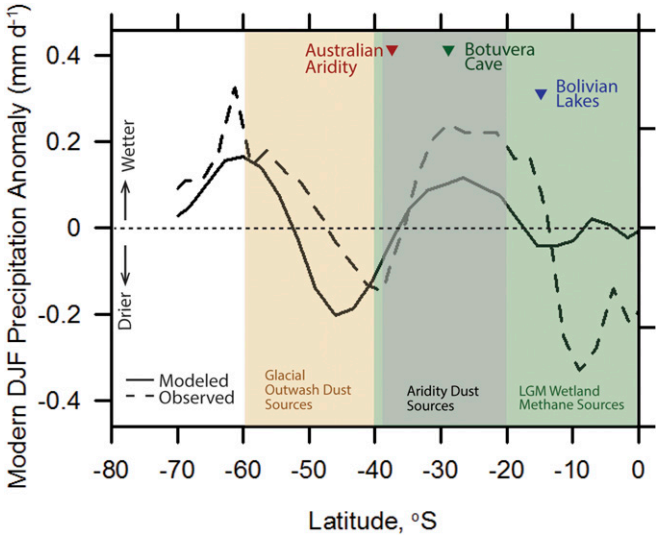

Fig. 5. Observed and modeled SH precipitation anomalies linked to modern stratospheric ozone depletion. Shown are observed and modeled zonal mean austral summer (DJF) net precipitation changes between 1979 and 2000 (37). Changes represent a ∼10% increase between 15°S and 35°S relative to the climatology (37). Simulated LGM responses to stratospheric ozone depletion are qualitatively similar (*SI Appendix, AOGCM Simulations*). Approximate latitude ranges for SH aridity and glacial outwash dust sources as well as wetlands during the LGM are indicated. Sharp changes in SH climate proxies occur exactly at this time (4, 6, 7, 10, 11, 14) (Fig. 1).

modern ozone hole. These simulations include surface warming of 0.4 °C to 0.8 °C over all of Antarctica and the Southern Ocean, in agreement with quasi-equilibrium simulations of the modern ozone hole (39, 40) (*SI Appendix, AOGCM Simulations*). These longer-term surface temperature responses are separate from the initial cooling simulated for modern stratospheric ozone depletion (41).

Previous studies (e.g., ref. 42) suggested that rising insolation initiated melting of Northern Hemisphere (NH) ice sheets at 19 ka, which triggered a reduction in the strength of the Atlantic overturning circulation, and, through the bipolar seesaw, resulted in SH warming and CO_2 release from the Southern Ocean, although the exact mechanisms driving the CO_2 release are still debated. We postulate that the ∼192-y series of halogen-rich eruptions of Mount Takahe and the subsequent ozone hole (26) initiated a series of events analogous to the modern ozone hole that acted to accelerate deglaciation at 17.7 ka. First, stratospheric ozone depletion changed SH atmospheric circulation, resulting in a rapid increase and poleward shift in the westerlies (35) (*SI Appendix*, Fig. S7). Second, consequent widespread perturbations in SH hydrometeorology, including increased austral summer subtropical precipitation between ∼15°S and ∼35°S (Figs. 1*F* and 5), led to enhanced CH_4 wetland emissions (43). Third, the combination of increased subtropical and decreased midlatitude precipitation, lower wind speeds between ∼35°S and ∼50°S (Fig. 5) (8, 37, 44), and warming centered at ∼60°S (35) (*SI Appendix*, Fig. S7), altered climate throughout SH LGM dust source regions (45). The result was a pronounced, synchronous, ∼50% decline in SH dust deposition (Fig. 1), reducing ocean biological uptake (10, 46) and thereby sharply reducing the ocean CO_2 sink. In Patagonia and New Zealand, warmer and dryer conditions south of ∼35°S (37) led to the well-documented retreat of glaciers (4–6) that starved glacial outwash plains of their fine-sediment resupply (45), with lower wind speeds possibly also contributing to reduced dustiness (47). In aridity-driven SH dust source regions located north of ∼35°S (Australia, Africa, extratropical South America), a cooler and wetter climate (37) sharply reduced aridity and hence dust export (9). Fourth, westerlies shifted poleward (*SI Appendix*, Fig. S8) and thus altered sea ice extent, leading to changes in upwelling of deep ocean carbon and nutrients, particularly in austral summer when, because of minimal sea ice and generally lower wind speeds, impacts on the carbon cycle were most pronounced (48). The net effect of these physical and biological pumps on the carbon cycle (16) likely started the release of CO_2 and initiated the rise in atmospheric CO_2 that followed the 17.7 ka Mount Takahe Event (Fig. 1) (14, 15). As with modern increases in greenhouse gases (49), the atmospheric and oceanic circulation as well as hydroclimatic changes initiated by stratospheric ozone depletion were reinforced by rising CO_2 (15) and CH_4 (12, 16).

Conclusion

Although the climate system already was primed for the switch from a glacial to interglacial state by insolation changes (1) and NH land ice loss (42), the ∼192-y ozone hole resulting from the halogen-rich eruptions of Mount Takahe plausibly provided supplementary forcing during the last termination that drove the westerly wind belt poleward and altered SH hydroclimate, providing a straightforward explanation for the synchronicity and abruptness of the SH climatic changes and global greenhouse gases that occurred ∼17.7 ka.

Materials and Methods

Ice Core Measurements. A nearly contiguous set of longitudinal WD samples from 1,300 m to 2,710 m depth was analyzed using a state-of-the-art continuous ice core analytical system (50–53) (*SI Appendix*, Fig. S8), in addition to replicate WD samples from 2,419.3 m to 2,435.2 m and all samples of the Byrd core (17) available from the University of Copenhagen archive between 1,242.06 ma and 1,303.39 m depth (*SI Appendix, Continuous Ice Core Measurements*). Samples from Taylor Glacier in the Antarctic Dry Valleys (54) also provided a record of the Mount Takahe event (Fig. 3). Additional measurements, including fluoride, bromide, and methane sulfonic acid, were made on discrete samples (*SI Appendix, Discrete Ice Core Measurements*).

Sulfur isotopes were measured on selected discrete samples using multicollector inductively coupled plasma mass spectrometry (ICP-MS) (55). The measured isotopic ratios were converted to δ values (Vienna-Canyon Diablo Troilite) using the International Atomic Energy Agency standards S5 and S6 and the standard NBS127. The $\delta^{34}S$ and $\delta^{33}S$ values of $NaSO_4$ ($\Delta^{33}S = 0$) were used to calibrate the instrument. The instrumental uncertainty for $\Delta^{33}S$, defined as 2 times the SD (2σ) of replicate measurement of the internal standards, was ±0.42‰. Volcanic events in ice cores previously sampled for sulfur isotope studies contained volcanic sulfur concentrations typically 3- to 10-fold greater than background sulfur concentrations (31, 32). Sulfur concentrations during the 17.7 ka event were only 1.7 times background (Fig. 4).

In a reinterpretation of the original Byrd core measurements (17), LaViolette (21) proposed an extraterrestrial origin. Helium (He), and especially ^3He, is much higher in extraterrestrial matter than in terrestrial components (56). Approximately 3 kg of discrete meltwater samples were collected from the outer ring of the melter head for He concentration and isotope measurements above, within, and below the 17.7 ka event. Average ^3He concentrations were 4.4e-17 (±2.5e-17) $cm^3 \cdot g^{-1}$ and 3.7e-17 (±2.5e-17) $cm^3 \cdot g^{-1}$ in the five background and four 17.7 ka event samples, respectively. Similarly, the $^3He/^4He$ ratios were 6.8e-5 (±1.7e-5) in the background samples and 7.3e-5 (±1.9e-5) in the event samples. Interplanetary dust fluxes calculated from these data were in agreement with past measurements (57), indicating no evidence for an extraterrestrial source for the 17.7 ka anomaly.

Volcanic Tephra Measurements. Insoluble tephra particles were captured on 10-μm stainless steel filters during continuous analyses for a background section of WD ice with no chemical evidence of volcanic fallout, as well as two sets of filters representing the early and later stages during the extended volcanic period (*SI Appendix*, Fig. S8). Additional tephra was filtered from larger-volume, discrete samples collected as part of targeted replicate coring at WD (*SI Appendix, Tephra Sampling and Geochemistry*).

Small concentrations of silicate particles were detected for the depth interval corresponding to the early stages of the 17.7 ka event (2,430 m to 2,426 m). No glass shards were found in the background sample or in the sample corresponding to the later stages of the 17.7 ka event, consistent with the continuous

insoluble particle measurements (*SI Appendix*, Fig. S1). Most of the particles identified in the sample were fine (~10 μm), and some had cuspate shapes suggestive of volcanic origin. Quantitative geochemical analysis of the particles indicates the presence of volcanic glass with an iron-rich trachytic composition characteristic of West Antarctic volcanism (*SI Appendix*, Table S1). The two main eruptive source volcanoes in West Antarctica, Mount Takahe (76°18.8′S, 112°4.8′W) and Mount Berlin (76°3′S, 136°0′W), are located 350 km north and 670 km northwest of the WD drilling site, respectively. The composition of tephra erupted from these two volcanoes is similar but can be distinguished by examining the MgO content of the volcanic glass, which is significantly higher in Mount Takahe eruptions (up to 0.5 wt.%) than in Mount Berlin eruptions, many of which have undetectable levels of MgO (24, 58).

Break Point Estimates. The break function regression algorithm BREAKFIT (59) was used to estimate the timing and uncertainty (1σ) of concentration changes in nssCa, CH_4, and CO_2 (Fig. 2). Intersecting linear trends were fit to nssCa and CH_4 measurements corresponding to 17.0 ka to 20.0 ka, and CO_2 measurements corresponding to 16.0 ka to 20.0 ka. Estimated break points for nssCa and CH_4 were 17.882 ka (±0.179 ka) and 17.759 ka (±0.075 ka), respectively. Similarly, the break point for CO_2 was 17.612 ka (±0.051 ka).

ACKNOWLEDGMENTS. We acknowledge R. von Glasow for help with snowpack model simulations, and J. Stutz and R. Kreidberg for helpful discussions. The US National Science Foundation supported this work [Grants 0538427, 0839093, and 1142166 (to J.R.M.); 1043518 (to E.J.B.); 0538657 and 1043421 (to J.P. Severinghaus); 0538553 and 0839066 (to J.C.-D.); and 0944348, 0944191, 0440817, 0440819, and 0230396 (to K.C.T.)]. We thank the WAIS Divide Science Coordination Office and other support organizations. P.K. and G.K. were funded by Polar Regions and Coasts in a Changing Earth System-II, with additional support from the Helmholtz Climate Initiative.

1. Hays JD, Imbrie J, Shackleton NJ (1976) Variations in Earth's orbit - Pacemaker of ice ages. *Science* 194:1121–1132.
2. Cheng H, et al. (2009) Ice age terminations. *Science* 326:248–252.
3. Landais A, et al. (2013) Two-phase change in CO_2, Antarctic temperature and global climate during Termination II. *Nat Geosci* 6:1062–1065.
4. Boex J, et al. (2013) Rapid thinning of the late Pleistocene Patagonian Ice Sheet followed migration of the Southern Westerlies. *Sci Rep* 3:2118.
5. Moreno P, et al. (2015) Radiocarbon chronology of the Last Glacial Maximum and its termination in northwestern Patagonia. *Quat Sci Rev* 122:233–249.
6. Putnam A, et al. (2013) Warming and glacier recession in the Rakaia valley, Southern Alps of New Zealand, during Heinrich Stadial 1. *Earth Planet Sci Lett* 382:98–110.
7. Placzek C, Quade J, Patchett PJ (2006) Geochronology and stratigraphy of late Pleistocene lake cycles on the southern Bolivian Altiplano: Implications for causes of tropical climate change. *Geol Soc Am Bull* 118:515–532.
8. Cruz FW, Jr, et al. (2005) Insolation-driven changes in atmospheric circulation over the past 116,000 years in subtropical Brazil. *Nature* 434:63–66.
9. De Deckker P, Moros M, Perner K, Jansen E (2012) Influence of the tropics and southern westerlies on glacial interhemispheric asymmetry. *Nat Geosci* 5:266–269.
10. Martínez-García A, et al. (2014) Iron fertilization of the Subantarctic ocean during the last ice age. *Science* 343:1347–1350.
11. Lambert F, et al. (2008) Dust-climate couplings over the past 800,000 years from the EPICA Dome C ice core. *Nature* 452:616–619.
12. WAIS Divide Project Members (2013) Onset of deglacial warming in West Antarctica driven by local orbital forcing. *Nature* 500:440–444.
13. Cuffey KM, et al. (2016) Deglacial temperature history of West Antarctica. *Proc Natl Acad Sci USA* 113:14249–14254.
14. Schmitt J, et al. (2012) Carbon isotope constraints on the deglacial CO_2 rise from ice cores. *Science* 336:711–714.
15. Marcott SA, et al. (2014) Centennial-scale changes in the global carbon cycle during the last deglaciation. *Nature* 514:616–619.
16. Völker C, Köhler P (2013) Responses of ocean circulation and carbon cycle to changes in the position of the Southern Hemisphere westerlies at Last Glacial Maximum. *Paleoceanography* 28:726–739.
17. Hammer CU, Clausen HB, Langway CC (1997) 50,000 years of recorded global volcanism. *Clim Change* 35:1–15.
18. Sigl M, et al. (2016) The WAIS Divide deep ice core WD2014 chronology - Part 2: Annual-layer counting (0-31 ka BP). *Clim Past* 12:769–786.
19. Neumann TA, et al. (2008) Holocene accumulation and ice sheet dynamics in central West Antarctica. *J Geophys Res Earth Surf* 113:9.
20. Matsumoto A, Hinkley TK (2001) Trace metal suites in Antarctic pre-industrial ice are consistent with emissions from quiescent degassing of volcanoes worldwide. *Earth Planet Sci Lett* 186:33–43.
21. LaViolette PA (2005) Solar cycle variations in ice acidity at the end of the last ice age: Possible marker of a climatically significant interstellar dust incursion. *Planet Space Sci* 53:385–393.
22. Francis P, Burton MR, Oppenheimer C (1998) Remote measurements of volcanic gas compositions by solar occultation spectroscopy. *Nature* 396:567–570.
23. Wardell LJ, Kyle PR, Counce D (2008) Volcanic emissions of metals and halogens from White Island (New Zealand) and Erebus volcano (Antarctica) determined with chemical traps. *J Volcanol Geotherm Res* 177:734–742.
24. Wilch TI, McIntosh WC, Dunbar NW (1999) Late Quaternary volcanic activity in Marie Byrd Land: Potential Ar-40/Ar-39-dated time horizons in West Antarctic ice and marine cores. *Geol Soc Am Bull* 111:1563–1580.
25. Palais JM, Kyle PR, McIntosh WC, Seward D (1988) Magmatic and phreatomagmatic volcanic activity at Mt Takahe, West Antarctica, based on tephra layers in the Byrd ice core and field observations at Mt Takahe. *J Volcanol Geotherm Res* 35:295–317.
26. Kutterolf S, et al. (2013) Combined bromine and chlorine release from large explosive volcanic eruptions: A threat to stratospheric ozone? *Geology* 41:707–710.
27. Solomon S, et al. (2016) Emergence of healing in the Antarctic ozone layer. *Science* 353:269–274.
28. Ivy D, et al. (2017) Observed changes in the Southern Hemispheric circulation in May. *J Clim* 30:527–536.
29. Cadoux A, Scaillet B, Bekki S, Oppenheimer C, Druitt TH (2015) Stratospheric ozone destruction by the Bronze-Age Minoan eruption (Santorini Volcano, Greece). *Sci Rep* 5:12243.
30. Patris N, Delmas RJ, Jouzel J (2000) Isotopic signatures of sulfur in shallow Antarctic ice cores. *J Geophys Res Atmos* 105:7071–7078.
31. Baroni M, Thiemens MH, Delmas RJ, Savarino J (2007) Mass-independent sulfur isotopic compositions in stratospheric volcanic eruptions. *Science* 315:84–87.
32. Savarino J, Romero A, Cole-Dai J, Thiemens MH (2003) UV induced mass-independent sulfur composition in stratospheric volcanic eruptions. *Geochim Cosmochim Acta* 67: A417–A417.
33. Abbatt JPD, et al. (2012) Halogen activation via interactions with environmental ice and snow in the polar lower troposphere and other regions. *Atmos Chem Phys* 12: 6237–6271.
34. Thomas JL, et al. (2011) Modeling chemistry in and above snow at Summit, Greenland - Part 1: Model description and results. *Atmos Chem Phys* 11:4899–4914.
35. Thompson DWJ, et al. (2011) Signatures of the Antarctic ozone hole in Southern Hemisphere surface climate change. *Nat Geosci* 4:741–749.
36. Polvani LM, Waugh DW, Correa GJP, Son S-W (2011) Stratospheric ozone depletion: The main driver of twentieth-century atmospheric circulation changes in the Southern Hemisphere. *J Clim* 24:795–812.
37. Kang SM, Polvani LM, Fyfe JC, Sigmond M (2011) Impact of polar ozone depletion on subtropical precipitation. *Science* 332:951–954.
38. Waugh DW, Primeau F, Devries T, Holzer M (2013) Recent changes in the ventilation of the southern oceans. *Science* 339:568–570.
39. Bitz CM, Polvani LM (2012) Antarctic climate response to stratospheric ozone depletion in a fine resolution ocean climate model. *Geophys Res Lett* 39:L20705.
40. Ferreira D, Marshall J, Bitz C, Solomon S, Plumb A (2015) Antarctic Ocean and sea ice response to ozone depletion: A two-time-scale problem. *J Clim* 28:1206–1226.
41. Solomon A, Polvani L, Smith K, Abernathey R (2015) The impact of ozone depleting substances on the circulation, temperature, and salinity of the Southern Ocean: An attribution study with CESM1(WACCM). *Geophys Res Lett* 42:5547–5555.
42. Shakun JD, et al. (2012) Global warming preceded by increasing carbon dioxide concentrations during the last deglaciation. *Nature* 484:49–54.
43. Baumgartner M, et al. (2012) High-resolution interpolar difference of atmospheric methane around the Last Glacial Maximum. *Biogeosciences* 9:3961–3977.
44. Gonzalez PM, Polvani L, Seager R, Correa GP (2013) Stratospheric ozone depletion: A key driver of recent precipitation trends in South Eastern South America. *Clim Dyn* 42: 1775–1792.
45. Sugden DE, McCulloch RD, Bory AJM, Hein AS (2009) Influence of Patagonian glaciers on Antarctic dust deposition during the last glacial period. *Nat Geosci* 2:281–285.
46. Bauska TK, et al. (2016) Carbon isotopes characterize rapid changes in atmospheric carbon dioxide during the last deglaciation. *Proc Natl Acad Sci USA* 113:3465–3470.
47. Mcgee D, Broecker W, Winckler G (2010) Gustiness: The driver of glacial dustiness? *Quat Sci Rev* 29:2340–2350.
48. Hauck J, et al. (2013) Seasonally different carbon flux changes in the Southern Ocean in response to the southern annular mode. *Global Biogeochem Cycles* 27:1236–1245.
49. Son SW, et al. (2008) The impact of stratospheric ozone recovery on the Southern Hemisphere westerly jet. *Science* 320:1486–1489.
50. McConnell JR, et al. (2014) Antarctic-wide array of high-resolution ice core records reveals pervasive lead pollution began in 1889 and persists today. *Sci Rep* 4:5848.
51. Sigl M, et al. (2015) Timing and climate forcing of volcanic eruptions for the past 2,500 years. *Nature* 523:543–549.
52. Maselli OJ, et al. (2017) Sea ice and pollution-modulated changes in Greenland ice core methanesulfonate and bromine. *Clim Past* 13:39–59.
53. McConnell JR, Edwards R (2008) Coal burning leaves toxic heavy metal legacy in the Arctic. *Proc Natl Acad Sci USA* 105:12140–12144.
54. Baggenstos D (2015) Taylor Glacier as an archive of ancient ice for large-volume samples: Chronology, gases, dust, and climate. PhD thesis (Univ Calif, San Diego).
55. Paris G, Sessions AL, Subhas AV, Adkins JF (2013) MC-ICP-MS measurement of delta S-34 and Delta S-33 in small amounts of dissolved sulfate. *Chem Geol* 345:50–61.
56. Farley KA, Mukhopadhyay S (2001) An extraterrestrial impact at the Permian-Triassic boundary? *Science* 293:2343.
57. Winckler G, Fischer H (2006) 30,000 years of cosmic dust in Antarctic ice. *Science* 313:491.
58. Dunbar NW, McIntosh WC, Esser RP (2008) Physical setting and tephrochronology of the summit caldera ice record at Mount Moulton, West Antarctica. *Geol Soc Am Bull* 120:796–812.
59. Mudelsee M (2009) Break function regression. *Eur Phys J Spec Top* 174:49–63.
60. Rhodes RH, et al. (2015) Paleoclimate. Enhanced tropical methane production in response to iceberg discharge in the North Atlantic. *Science* 348:1016–1019.